Energy shell structure in a dielectric elliptic microcavity

Chang-Hwan Yi,[1,*] Hyeon-Hye Yu,[2] Ji-Won Lee,[1] Ji-Hwan Kim,[1] and Chil-Min Kim[1,†]

[1]*Department of Emerging Materials Science, DGIST, Hyeonpung-myeon, Dalseong-gun, Daegu 711-873, Korea*
[2]*Department of Physics, Sogang University, Seoul 121-742, Korea*

An energy shell structure depending on eccentricity is analyzed in a dielectric elliptic microcavity. Through the analysis, it is explicated that the energy shell structure is governed by classical constant actions of periodic orbits. For clarification, the relation between dominances of the periodic orbits and bifurcation behaviors are obtained and the length spectra based on eigenvalues computed by a numerical method are compared with the exact lengths of the periodic orbits obtained by analytic calculations. By matching effective wave numbers obtained from the periodic orbit lengths to exact wave numbers of stationary states in closed and open cavities, we find deviations provoked from the openness. We show that these deviations are caused by additional phase factors in the Einstein-Brillouin-Keller quantization.

I. INTRODUCTION

Unidirectionally emitting high-Q dielectric microcavities are considered as one of the most promising candidates for a light source in optoelectric circuits [1,2]. Up to now, various cavity shapes have been reported for the achievement of those microcavities [3,4]. However, both the properties of high Q and directionality cannot be accomplished at once without understanding the mode structure depending on deformation, because while modes in symmetric cavities cannot exhibit directionality, those in asymmetric cavities hardly have high-Q factors [5,6]. In addition, since the morphological characteristics of modes are dynamically changed depending on deformation due to interactions of the modes [7,8], optimization of the parameter value satisfying the two properties is not a trivial task. Therefore, it is indeed a crucial gateway not to deviate from investigating the mode structures depending on the parameters, i.e., the energy level structures.

The energy level structures have been studied in various fields, such as metallic clusters [9], nuclei [10,11], atoms [12], quantum dots [13–15], molecules [16], and billiards [10,11,14,15,17,18]. The term "energy shell structure," which depicts the energy level structure in such systems as enumerated above, comes from the fact that the individual energy levels do not exhibit equidistant spacings, but rather gather together in a bunch, clustering with approximately the same distances. In these studies, the actions of periodic orbits perform a crucial role in calculating the density of states [18–20]. The principle goal in this calculation is to understand the energy shell structures by using semiclassical methods. Because the density of states has a monotonically increasing smooth part (Thomas-Fermi approximation or Weyl's law) and an oscillating part [14,18,21], practically, the studies aim to obtain the oscillating part of the density of states under static conditions (i.e., under the conditions that no parametric variation is conducted). On the other hand, in the study of the dynamical properties of the energy level states, the actions are conceived to be the invariant variables which are preserved under slow parametric variations [22–28]. The two concepts, energy shell structure and constant action, can be bound together through the Einstein-Brillouin-Keller (EBK) quantization, which is the action quantization [29,30].

In this paper, we will investigate parameter dependent eigenvalues in dielectric elliptic microcavities, open systems, in order to reveal how the constant actions, i.e., the adiabatic invariants, of the periodic orbits can govern the variations of the eigenvalues depending on eccentricity. Because the eigenvalues of the open systems are complex values, the energy shell structure is detuned from those of the closed ones. When we apply additional phase factors to the EBK quantization, these detunings, i.e., deviations from the closed systems, are compensated and agree well with adiabatic invariant curves (constant action curves).

The energy shell structure of the elliptic dielectric microcavity is analyzed first by the Fourier transform of a density of states, which is referred to as the length spectrum [10,31,32]. In the analysis, the correspondence between the adiabatic invariants and the energy shell structures is confirmed by matching the lengths of dominant short periodic orbits [10,15] to the length spectrum. A direct demonstration of the correspondence between the effective wave numbers that are proportional to the inverse length of the periodic orbits and the energy shell structures is given at the end of the paper. Also, we elucidate the causes of deviations between the billiard and dielectric systems with respect to the shell structures. While the densities of states in both systems have the same free spectral ranges [33] for the dominant dense lines in the spectra, the shell structure of the dielectric cavity does not coincide with the adiabatic invariant lines of the periodic orbits. Hence, we perform corrections of these deviations by inserting additional phase factors, induced by the Fresnel law, to the EBK quantization in obtaining the effective wave numbers.

II. ACTIONS OF PERIODIC ORBIT IN ELLIPTIC COORDINATE

The boundary of an elliptic cavity is given as follows,

$$x^2 + \frac{y^2}{1 - \varepsilon^2} = a^2, \tag{1}$$

where a is the semimajor radius and ε is eccentricity given such that $\varepsilon = \sqrt{1 - b^2/a^2}$. In an ellipse, two foci are defined such that $f = \pm a\varepsilon$ and the semiminor radius is $b = \sqrt{a^2 - f^2}$. In obtaining the energy shell structure, i.e., the energy level structure, the cavity area is preserved as eccentricity increases such that $\pi ab = \pi$. Depending on eccentricity, the eigenvalues of the Helmholtz equation are obtained by using the standard numerical method [34], or more originally [35].

In order to explore the energy shell structure of an elliptic cavity, first, the actions of periodic orbits are deduced. Among many current approaches, our discussions are based mainly on those of Ref. [36]. It is known that the shorter periodic orbits dominantly contribute to the shell structure [10]. To obtain the actions, the periodic orbit in the Cartesian coordinate is transformed into that in an elliptic coordinate by using the following relations,

$$x = f \cosh u \cos v, \quad y = f \sinh u \sin v, \quad (2)$$

where the symbols u and v are the hyperbolic and the elliptic axes, respectively. In an elliptic coordinate, we can obtain two conserved quantities, the Hamiltonian and the product of two angular momenta with respect to the two foci, as follows,

$$H = \frac{p_u^2 - p_v^2}{f^2(\cosh^2 u - \cos^2 v)}, \quad (3)$$

$$L_1 L_2 = \frac{p_u^2 \sinh^2 u - p_v^2 \sin^2 v}{\cosh^2 u - \cos^2 v}, \quad (4)$$

where p_u and p_v are the momenta on the hyperbolic and the elliptic axes, respectively. Here, the mass is assumed to be $1/2$ for the sake of convenience. Because the Hamiltonian, i.e., the energy E, and the product of two angular momenta $L_1 L_2$ with respect to the two foci are the conserved quantities in an elliptic shaped Hamiltonian system, by defining the quantity $\alpha = L_1 L_2 / E$, we can obtain the canonical momenta expediently as follows:

$$p_u^2 = E(f^2 \sinh^2 u - \alpha), \quad p_v^2 = E(f^2 \sin^2 v + \alpha). \quad (5)$$

From the momenta, we can obtain the actions with respect to the hyperbolic (u) and the elliptic (v) degrees of freedom as follows:

$$I_u = \frac{1}{2\pi} \oint p_u du = \frac{\sqrt{E}}{\pi} \int_{u_s}^{u_e} du \sqrt{f^2 \sinh^2 u - \alpha}, \quad (6)$$

$$I_v = \frac{1}{2\pi} \oint p_v dv = \frac{2\sqrt{E}}{\pi} \int_{v_s}^{v_e} dv \sqrt{f^2 \sin^2 v + \alpha}. \quad (7)$$

In Eqs. (6) and (7), the upper and the lower limits of the integrals are deduced by the value α [36], which divides the motion characteristics of orbits into a whispering gallery type (WG type) and a libration motion type (LM type). When $-f^2 < \alpha < 0$, the motion is of a LM type and when $0 < \alpha < b^2$, it is of a WG type.

Because the actions for the periodic orbits are proportional to the total length of orbits such that $2\pi I = \oint p dq = \hbar k l_{\text{PO}} = 2\pi\hbar(N + \mu/4)$, a length $l_{\text{PO}}^{n,m}$ of periodic obit is defined as follows,

$$l_{\text{PO}}^{n,m} = \frac{2\pi}{\sqrt{E}}(nI_u + mI_v), \quad (8)$$

where n and m are the cycling numbers of each action variable I_u and I_v, respectively, and N, μ, and $\sqrt{E}$ are an integer, the Maslov index, and $\hbar k$, respectively. For the cycling numbers, in Eq. (8) above, n is the number of reflections on the system boundary, and m is the number of rotations and librations for the WG type and the LM type, respectively. The periodic conditions which are obtained by the winding number $\frac{n}{m}$ are given as follows,

$$\mathcal{F}\left(\sin^{-1}\sqrt{\frac{b^2 - \alpha}{b^2}}, \kappa\right) = \frac{2m}{n}\mathcal{F}\left(\frac{\pi}{2}, \kappa\right), \quad \alpha > 0, \quad (9)$$

$$\mathcal{F}\left(\sin^{-1}\sqrt{\frac{b^2}{b^2 - \alpha}}, \frac{1}{\kappa}\right) = \frac{2m}{n}\mathcal{F}\left(\frac{\pi}{2}, \frac{1}{\kappa}\right), \quad \alpha < 0, \quad (10)$$

and thus we can obtain the following results:

$$l_{\text{PO}}^{n,m} = \frac{2na}{b}\sqrt{b^2 - \alpha} - \frac{2nf}{\kappa}\mathcal{Z}\left(\frac{2m\mathcal{F}\left(\frac{\pi}{2}, \kappa\right)}{n}\right), \quad \alpha > 0,$$

$$l_{\text{PO}}^{n,m} = \frac{2nab}{\sqrt{b^2 - \alpha}} - 2nf\mathcal{Z}\left(\frac{2m\mathcal{F}\left(\frac{\pi}{2}, \frac{1}{\kappa}\right)}{n}\right), \quad \alpha < 0.$$

Here, $\mathcal{Z}(u) = \mathcal{E}(\phi, \kappa) - \mathcal{F}(\phi, \kappa)\frac{\mathcal{E}(\pi/2, \kappa)}{\mathcal{F}(\pi/2, \kappa)}$, $\mathcal{F}(\phi, \kappa)$, and $\mathcal{E}(\phi, \kappa)$ are the Jacobi zeta function, the elliptic integral of the first kind, and the elliptic integral of the second kind, respectively. The parameter κ is given by $\kappa = f/\sqrt{f^2 - \alpha}$.

By using the above equations, now we can obtain the length of the classical periodic orbits. Figure 1 is $1/l_{\text{PO}}^{n,m}$ depending on the eccentricity, which shows the bifurcations of periodic orbits. The bifurcation of periodic orbits in an elliptic cavity is well addressed in Ref. [32]. As a circular cavity deforms into an elliptic cavity, two kinds of distinct bouncing-ball-type orbits
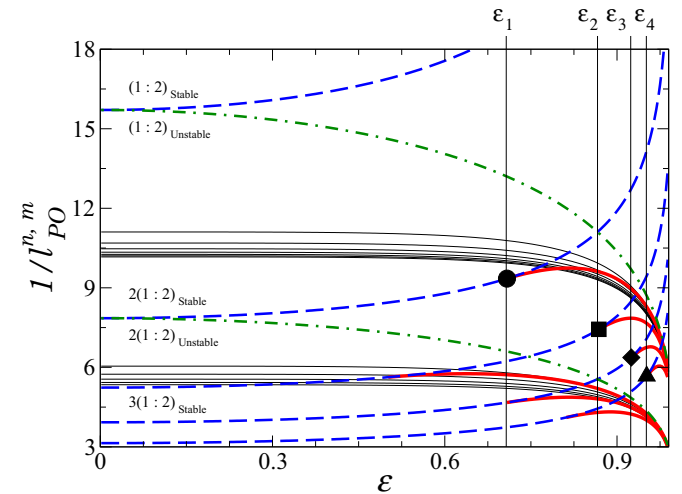

FIG. 1. Bifurcation diagram depending on eccentricity. The dashed lines are $1/l_{\text{PO}}^{n,m}$ of the short diametric orbits, which have a repetition multiplicity r, i.e., $r(1:2)$. The dotted dashed lines are those of the long diametric orbits. ε_1, ε_2, ε_3, and ε_4 are the bifurcation points of the periodic orbits such that $(m:n) = (1:4), (1:6), (1:8)$, and $(1:10)$, respectively. The points are $\varepsilon_1 \approx 0.707$, $\varepsilon_2 \approx 0.866$, $\varepsilon_3 \approx 0.924$, and $\varepsilon_4 \approx 0.952$. The thick solid lines are bifurcated periodic orbits. The thin lines are the whispering-gallery-type periodic orbits.

begin to appear. The bouncing-ball-type orbits of $(1:2)_{stab}$ and $(1:2)_{unst}$ are the orbits bouncing twice at the system boundary along the minor axis (stable) and the major axis (unstable) for one period, respectively. These primary orbits are maintained independent of eccentricity. The $2(1:2)_{stab}$ and $2(1:2)_{unst}$ are the orbits bouncing the minor and the major axes four times for a period, respectively. Between the two orbits, only the $2(1:2)_{stab}$ orbit (LM type) generates a bowtie-type $(1:4)$ orbit at the bifurcation point $\varepsilon_1 \approx 0.707$, as marked by a dashed blue and a solid red line in the figure. The $3(1:2)_{stab}$ and the $3(1:2)_{unst}$ are the orbits bouncing the minor and the major axes six times for a period, respectively, and only the $3(1:2)_{stab}$ orbit generates a candy-shaped $(1:6)$ orbit (see Fig. 4) at the bifurcation point $\varepsilon_2 \approx 0.866$. Similarly, various orbits (LM type) are generated by bifurcations. Each bifurcation point is as follows [32,36]:

$$\varepsilon = \cos \frac{m\pi}{n}. \qquad (11)$$

According to the above equation, each of the LM-type periodic orbits have their own bifurcation point. Examples are illustrated in Fig. 1 as marked by a solid circle for the $(1:4)$ periodic orbit, a solid square for $(1:6)$, a solid diamond for $(1:8)$, and a solid triangle for $(1:10)$, respectively.

III. LENGTH SPECTRUM AND ORBIT LENGTH

Next, in order to compare the length spectrum in the open elliptic cavity and the lengths of periodic orbits, a length spectrum is obtained which is based on the complex eigenvalues calculated by the boundary element method (BEM) [34]. The

lengths of the periodic orbits are given by Eq. (8). The resonant wave numbers, i.e., the complex eigenvalues, are obtained by solving the Helmholtz equation in the range $\mathcal{N}_e k R \leqslant 49$ when the effective refractive index $\mathcal{N}_e$ is 3.3. From the solutions, we can obtain a so-called *length spectrum*, the analogy of the "inverse quantum chaology" extended to the integrable system [31]. Among many previous approaches, we take the formula used in Ref. [32], which is given as follows,

$$d(l) = \int dk \exp\left[-ikl\right] g(e) \exp\left[-\left(\frac{k}{\sqrt{2}k_c}\right)^2\right]$$

$$= \sum_i \frac{1}{\mathcal{A}k_i} \exp\left[-ik_i l - \left(\frac{k_i}{\sqrt{2}k_c}\right)^2\right], \qquad (12)$$

where $g(e)$ is the density of states and $k_c = k_{max}/\sqrt{2}$. Here, k_{max} is the maximum eigenvalue among the calculated eigenvalues. In the above equation, a Gaussian root mean square is used in order to smoothly reduce a high frequency effect. In numerical computations, the constant factor $\mathcal{A}$ is set to be unity without any loss of generality.

Using Eq. (12), we obtain the length spectrum in the parameter range $0 < \varepsilon < 0.95$. Figure 2 shows the length spectrum and the lengths of periodic orbits in the range $0.5 < \varepsilon < 0.95$. In Fig. 2(b), we can recognize the structure of the length spectrum in an open elliptic microcavity. In order to clarify the structure, we prepare periodic orbit lengths obtained from Eq. (8) depending on eccentricity, as illustrated in Fig. 2(a). To compare the two structures, the length spectrum at $\varepsilon = 0.8$ is superimposed on Fig. 2(a) as an example. In the figure, the peaks of the length spectrum at $\varepsilon = 0.8$ coincide
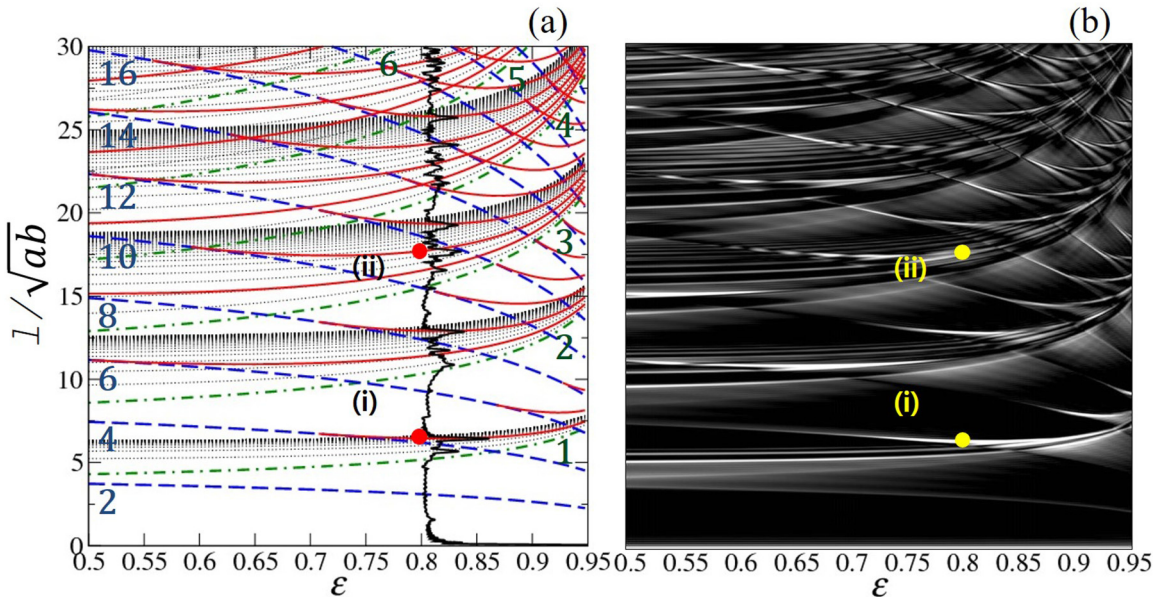

FIG. 2. Lengths of periodic orbits and amplitude of the length spectrum. (a) Orbit lengths obtained from Eqs. (2) and (3). (b) Amplitude of the length spectrum obtained from wave numbers. The white color is the maximum amplitude and the black is the minimum. The vertical axis is the dimensionless length of the periodic orbits and the horizontal axis is eccentricity. In (a), the left even numbers are the bouncing numbers on the boundary for a period and the right integer numbers are the rotation (libration) numbers of the orbits. The superimposed vertical one-dimensional (1D) graph in (a) is the selected length spectrum at $\varepsilon = 0.8$. Points (i) and (ii) are marked for the examples of periodic orbits, which are the $(1:4)$ and the $(3:10)$ orbits. In (a), the solid red lines are the lengths of the bifurcated LM-type orbits, the dashed blue lines are the lengths of the stable bouncing-ball-type orbits, the dotted dashed green lines are the lengths of the unstable bouncing-ball-type orbits, and the thin dotted black lines are the lengths of the WG-type orbits.
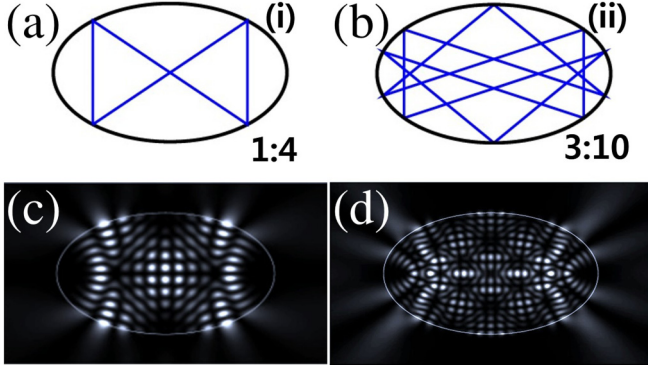
FIG. 3. Selected orbits and their wave functions. (a) and (c) are the (1 : 4) periodic orbit and the wave function localized on the periodic orbit, respectively. (b) and (d) are the (3 : 10) periodic orbit and the wave function localized on the orbit, respectively.

well with the lengths of the periodic orbits. This means that the background classical periodic orbits in the system substantially effect the quantum mechanical shell structures.

The (1 : 4) and the (3 : 10) periodic orbits at points (i) and (ii) in Fig. 2 are shown in Figs. 3(a) and 3(b), respectively. The wave functions localized on the (1 : 4) and the (3 : 10) periodic orbits are illustrated in Figs. 3(c) and 3(d), respectively. The wave functions shown in Figs. 3(c) and 3(d) are "scarlike" resonances.

The periodic orbit at point (i) is defined as follows: The red line is bifurcated from a short diametric orbit reflecting four times at around $\varepsilon \approx 0.707$ and its asymptotic line follows a long diametric orbit librating one time in the high deformation limit as $\varepsilon \to 1$. Hence, this orbit is the (1 : 4) periodic orbit.

In the same manner, point (ii) can be labeled by the (3 : 10) periodic orbit. This interesting feature, which is related to the bifurcation point and the asymptotic reunification to the other orbits, is analogous to the behaviors of bridge orbits in the nuclei system [10]. An analysis of this observation will be shown in future publications. Similarly, we can expect other bifurcated periodic orbits to appear in the wave-function morphology. As already stated above, all the LM-type periodic orbits have their own bifurcation points and can show up in an open system while the billiard cannot produce these orbits in the wave-function morphology.

Several wave functions localized on the periodic orbits, which are bifurcated from the bouncing-ball-type periodic orbits, are illustrated in Fig. 4. Figure 4(a) is the bouncing-

ball-type wave function. The wave function shown in Fig. 4(b) is localized on the (1 : 4) periodic orbit, which is bifurcated from the 2(1 : 2) periodic orbit. Similarly, the wave functions shown in Figs. 4(c)–4(e) are localized on the (1 : 6), (1 : 8), and (1 : 10) periodic orbits, which are bifurcated from the 3(1 : 2), 4(1 : 2), and 5(1 : 2) periodic orbits. This means that a (1 : 2t) periodic orbit is bifurcated from an t(1 : 2) periodic orbit, where t is an integer.

IV. ENERGY SHELL STRUCTURE

On the basis described above, now we study the energy shell structure of a dielectric elliptic microcavity. As we have shown an obvious correspondence between the eigenvalue based length spectrum and the classical periodic orbit length, we can expect a relation between the energy shell structure of a dielectric elliptic microcavity and the orbit lengths, although there is a substantial difference between an elliptic billiard and an open elliptic microcavity.

In an elliptic billiard, the energy shell structure is obtained by using BEM with the Dirichlet boundary condition. In a dielectric elliptic microcavity, the eigenvalues are obtained by using BEM with the transverse magnetic (TM) boundary condition, and the periodic orbits are quantized through the EBK quantization rule [10,32,37,38]. In a dielectric elliptic microcavity, mode coupling phenomena occur due to interactions between a pair of wave functions, which result in wave functions localized on periodic orbits. This is a kind of scarring phenomenon referred to as a scarlike resonance [39–42].

Figures 5(a) and 5(b) are the energy shell structures of an elliptic billiard and an open elliptic cavity in the region $0.5 < \varepsilon < 0.95$ and $34 < kR < 46$ for an elliptic billiard and in the region $0.5 < \varepsilon < 0.95$ and $34 < \mathrm{Re}(\mathcal{N}_e kR) < 46$ for a dielectric elliptic microcavity, respectively. The structures exhibit irregular densities depending on eccentricity, as depicted in Fig. 5. In both figures, we can recognize several sequences of equidistantly spaced line structures, which are distinctive in their high density. The equidistant spacing, i.e., the free spectral range of these structures, is responsible for the peaks of the length spectrum as discussed above, since the Fourier transform, in obtaining the length spectrum, demonstrates a period of equidistant lines [43,44]. Hence, we can conjecture that these lines should correspond to periodic orbit lengths, which are proportional to the actions.
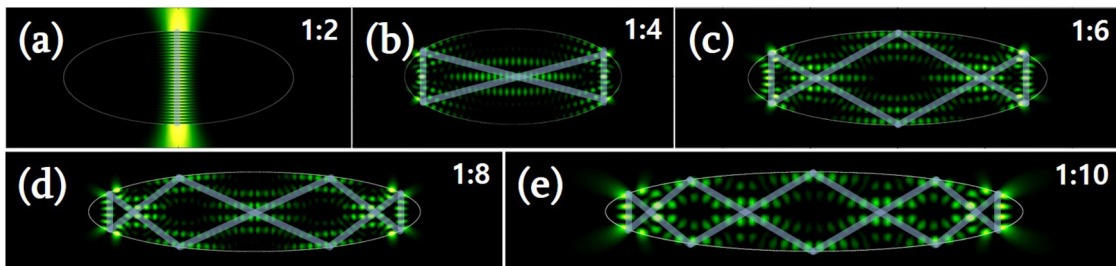

FIG. 4. Sequentially bifurcated wave functions localized on periodic orbits. The first column in the upper left is the example wave function corresponding to the short diametric orbit and others are bifurcated orbits from the repeating short diametric orbit.
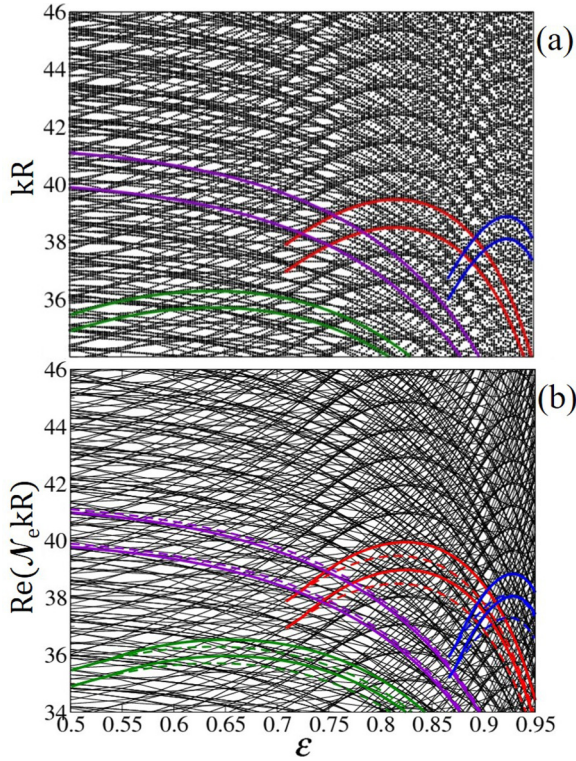
FIG. 5. Effective wave numbers obtained from constant actions, which are superimposed on the exact wave numbers. (a) is the billiard system and (b) is the dielectric system. Red, blue, green, and purple lines are the (1 : 4), (1 : 6), and (2 : 6) LM-type periodic orbits, and the (1 : 3) WG-type periodic orbit, which are ranged from $N = 37$ to 38, from 45 to 46, from 58 to 59, and from 33 to 34, respectively. Here, N is the quantum number.

By using the EBK quantization rule, the periodic orbit is quantized as follows [10,32,37,38],

$$(kR)_{\text{eff}} \equiv \frac{2\pi(N + \mu/4)}{l_{\text{PO}}} R, \qquad (13)$$

where μ is the Maslov index, which should be constructed depending on the characteristics of a periodic orbit. We obtain the effective wave numbers from a constant action $I = 2\pi(N + \mu/4)$ given by adequate integers N, μ and an estimated orbit length l_{PO} based upon the length spectrum in Fig. 2. The results are superimposed on both figures. As is shown in Fig. 5(a), in the case of a billiard, although there is no wave function localized on the periodic orbits, the dense lines agree well with the constant action curves.

In the case of the dielectric elliptic microcavity, however, the constant action curves (dashed lines) do not coincide with the exact eigenvalues obtained numerically, as shown in Fig. 5(b). This discrepancy is caused by the open property of the dielectric system which allows only quasibound states (i.e., the wave functions are not correctly positioned inside the system; instead, they are partially ranged on the system boundary with respect to both in and outside the system). This problem was already mentioned and discussed in Ref. [45], but the result was not illustrated explicitly. Furthermore, discussions in Ref. [45] were not focused on the parameter

dependent behaviors of the resonances. Therefore, now we will make up this discrepancy with explicit illustrations.

As stated above, the dielectric system does not allow vanishing wave functions on the system boundary because of openness; rather, it obeys the Fresnel reflection rules governed by the incident angle χ_i. The reflection coefficient can be the complex value when the incident angle is greater than the critical angle for total internal reflection. Therefore, when the reflection coefficient becomes the complex value, the reflection coefficient gives a phase shift to the reflected waves [33,46], and when this phase shift is taken into account, the complete form of the effective wave number for the dielectric system can be constructed,

$$(\mathcal{N}_e kR)_{\text{eff}} \equiv \frac{2\pi(N + \mu/4 + \phi_{\text{add}})}{l_{\text{PO}}} R, \qquad (14)$$

where

$$\phi_{\text{add}} = \text{Re}\left[-i \sum_{j=1}^{n} \ln\left(\frac{\mathcal{N}_e \cos\chi_i - \cos\chi_t}{\mathcal{N}_e \cos\chi_i + \cos\chi_t}\right)_j\right], \qquad (15)$$

$$\sin\chi_t = \mathcal{N}_e \sin\chi_i,$$

$$\chi_i = \sin^{-1}\left(\sqrt{\frac{\alpha + f^2 \sin^2 v}{b^2 + f^2 \sin^2 v}}\right). \qquad (16)$$

In Eq. (15), the sum is performed along the bouncing points of the periodic orbit from 1 to n. Since the periodic orbits in the ellipse exhibit a resonant torus, constituted by one parameter, i.e., α, a nonisolated periodic orbit family, the contribution of each periodic orbit should be averaged. For this purpose, we take 100 periodic orbits for each family, following Eq. (16). The results are truly satisfactory, as illustrated in Fig. 5(b) by thick solid lines, which are in a great coincidence with the dense lines of the background eigenvalue structures.

V. DISCUSSIONS AND CONCLUSION

The main idea of the analysis using Eq. (14) is based on an additional phase factor due to reflections on the interface between two materials, which have different refractive indices. Thus we believe that this idea also can be applicable to various integrable shapes of the microcavity, such as a rectangular and a triangular shape. However, out of concern for cavities having nonsmooth boundary curves, it is conjectured that we should pay much more careful attention to obtaining the phase factors when we deal with cavities exhibiting sharp corners, such as a rectangular cavity. In the case of the refractive index, it is reasonable to expect that Eq. (14) can hold for various refractive index cases, such as a polymer system ($\mathcal{N} = 1.5$). We have also checked the case of refractive index $\mathcal{N} = 2.0$ (not shown here) and have confirmed a consistency.

In the case of transverse electric (TE) polarization, though, the Brewster angle can significantly affect the additional phase factor, the trend of the real parts of complex eigenvalues that are not very different from those of TM polarization. Hence, we can expect a similar quantization rule for the TE polarization case. With respect to the imaginary parts of the resonances, it is hard to obtain an extended EBK quantization because we should attack this task along with couplings, interactions, and

a tunneling frameworks (avoided crossing behaviors of the imaginary parts of the resonances are much more complicated than those of the real one). Nevertheless, there were some trials [33,47] to obtain the quantization rule of the imaginary part of the resonances for some cavities, even though they were deduced without any kinds of interaction schemes. In future work, we will also try to resolve the problems of the quantization of resonances concerning the imaginary parts of the resonances.

In conclusion, we explicitly demonstrate that the constant action curves of the periodic orbits, which have been alternatively focused on as invariant quantities under adiabatic parametric variations, make significant contributions to the shell structures in the dielectric elliptic systems, by comparing the periodic orbit lengths and the length spectrum which is obtained by the Fourier transform of the density of states. The characteristics of the bifurcated periodic orbits are illustrated in order to clarify their roles in the shell structures depending on the parameter. The phase shift correction of the effective

wave numbers is also discussed, addressing the problem of the dielectric system. In the correction procedures, it is shown that an additional phase factor arises due to the complex reflectance. The resonant tori corresponding to periodic orbits partially gain this additional phase factor when the tori are located above the critical angle on the phase space. We believe that our results will provide a key to resolving the problems remaining in the field of quantum chaos and dissipating systems, which are fields undergoing intense study in the search for quantum signatures of classical chaos.

[1] *Optical Processes in Microcavities*, edited by R. K. Chang and A. J. Campillo (World Scientific, Singapore, 1996).

[2] *Optical Microcavities*, edited by K. Vahala (World Scientific, Singapore, 2004).

[3] H. Cao and J. Wiersig, Rev. Mod. Phys. **87**, 61 (2015), and references therein.

[4] T. Fukushima, T. Tanaka, and T. Harayama, Appl. Phys. Lett. **86**, 171103 (2005).

[5] J. U. Nöckel, A. D. Stone, and R. K. Chang, Opt. Lett. **19**, 1693 (1994).

[6] H. H. Yu, C. H. Yi, and C. M. Kim, Opt. Express **23**, 11054 (2015).

[7] H. G. L. Schwefel, N. B. Rex, H. E. Tureci, R. K. Chang, A. D. Stone, T. Ben-Messaoud, and J. Zyss, J. Opt. Soc. Am. B **21**, 923 (2004).

[8] C. H. Yi, H. H. Yu, J. W. Lee, and C. M. Kim, Phys. Rev. E **91**, 042903 (2015).

[9] W. A. de Heer, Rev. Mod. Phys. **65**, 611 (1993).

[10] K.-i. Arita, Phys. Rev. C **86**, 034317 (2012).

[11] V. M. Strutinsky, A. G. Magner, S. R. Ofengenden, and T. Døssing, Z. Phys. A **283**, 269 (1977).

[12] M. Kohout and A. Savin, Int. J. Quantum Chem. **60**, 875 (1996).

[13] S. Raymond *et al.*, Phys. Rev. Lett. **92**, 187402 (2004).

[14] M. Brack and R. K. Bhaduri, *Semiclassical Physics* (Addison-Wesley, New York, 1977).

[15] J. Blaschke and M. Brack, Phys. Rev. A **56**, 182 (1997).

[16] A. H. H. Chang, W. C. Ermler, and R. M. Pitzer, J. Phys. Chem. **95**, 9288 (1991).

[17] C. H. Yi, J. H. Kim, H. H. Yu, J. W. Lee, and C. M. Kim, Phys. Rev. E **92**, 022916 (2015).

[18] H. J. Stöckmann, *Quantum Chaos: An Introduction* (Cambridge University Press, London, 2000).

[19] M. C. Gutzwiller, J. Math. Phys. **12**, 343 (1971).

[20] R. Balian and C. Bloch, Ann. Phys. **64**, 271 (1971).

[21] R. Balian and C. Bloch, Ann. Phys. **69**, 76 (1972).

[22] J. W. S. Rayleigh, Philos. Mag. **3**, 338 (1902).

[23] *La Theorie du Rayonnement et les Quanta*, edited by P. Langevin and M. D. Broglie (Gauthier-Villars, Paris, 1912).

[24] W. P. Reinhardt, Prog. Theor. Phys. Suppl. **116**, 179 (1994).

[25] A. Einstein, Verh. d. Deutsch. Phys. Ges. **16**, 826 (1914); M. Jammer, *The Conceptual Development of Quantum Mechanics* (McGraw-Hill, New York, 1966).

[26] P. Ehrenfest, Ann. Phys. (Berlin) **51**, 327 (1916).

[27] P. Ehrenfest, Philos. Mag. **33**, 500 (1917).

[28] *Hamiltonian Dynamical Systems and Applications*, edited by W. Craig (Springer, Berlin, 2007).

[29] R. V. Lovelace, Phys. Fluids **22**, 542 (1979).

[30] E. Ott, Phys. Rev. Lett. **42**, 1628 (1979).

[31] H. Waalkens, J. Wiersig, and H. R. Dullin, Ann. Phys. **260**, 50 (1997).

[32] A. G. Magner *et al.*, Prog. Theor. Phys. **102**, 551 (1999).

[33] H. E. Tureci, H. G. L. Schwefel, E. E. Narimanov, and A. D. Stone, Opt. Express **10**, 752 (2002).

[34] J. Wiersig, J. Opt. A: Pure Appl. Opt. **5**, 53 (2003).

[35] P. A. Boasman, Nonlinearity **7**, 485 (1994).

[36] M. Sieber, J. Phys. A: Math. Gen. **30**, 4563 (1997).

[37] J. B. Keller and S. I. Rubinow, Ann. Phys. **9**, 24 (1960).

[38] L. J. Curtis and D. G. Ellis, Am. J. Phys. **72**, 1521 (2004).

[39] A. J. S. Traiber, A. J. Fendrik, and M. Bernath, J. Phys. A: Math. Gen. **22**, L365 (1989).

[40] J. Wiersig, Phys. Rev. Lett. **97**, 253901 (2006).

[41] J. Unterhinninghofen, J. Wiersig, and M. Hentschel, Phys. Rev. E **78**, 016201 (2008).

[42] C. H. Yi, S. H. Lee, M.-W. Kim, J. Cho, J. Lee, S. Y. Lee, J. Wiersig, and C.-M. Kim, Phys. Rev. A **84**, 041803(R) (2011).

[43] M. Lebental, N. Djellali, C. Arnaud, J. S. Lauret, J. Zyss, R. Dubertrand, C. Schmit, and E. Bogomolny, Phys. Rev. A **76**, 023830 (2007).

[44] E. Bogomolny, R. Dubertrand, and C. Schmit, Phys. Rev. E **78**, 056202 (2008).

[45] E. Bogomolny, N. Djellali, R. Dubertrand, I. Gozhyk, M. Lebental, C. Schmit, C. Ulysse, and J. Zyss, Phys. Rev. E **83**, 036208 (2011).

[46] G. R. Fowles, *Introduction to Modern Optics* (Dover, New York, 1975).

[47] M. Hentschel and J. U. Nöckel, arXiv:physics/0203064.